Journal of Alloys and Compounds 696 (2017) 1323–1328

Contents lists available at ScienceDirect

Journal of Alloys and Compounds

journal homepage: http://www.elsevier.com/locate/jalcom

New Fe-based amorphous soft magnetic composites with significant enhancement of magnetic properties by compositing with nano-$(NiZn)Fe_2O_4$

Li Xiaolong [a, b], Dong Yaqiang [a, *], Liu Min [a], Chang Chuntao [a, *], Wang Xin-Min [a]

[a] Zhejiang Province Key Laboratory of Magnetic Materials and Application Technology, Key Laboratory of Materials and Devices, Ningbo Institute of Materials Technology and Engineering, Chinese Academy of Sciences, Ningbo, 315201, China
[b] Nano Science and Technology Institute, University of Science and Technology of China, Hefei, Anhui, 230026, China

ARTICLE INFO

Article history:
Received 30 August 2016
Received in revised form
18 November 2016
Accepted 19 November 2016
Available online 20 November 2016

Keywords:
Amorphous powder
Amorphous soft magnetic composites
Insulation coating
Soft magnetic properties

ABSTRACT

Amorphous soft magnetic composites based on spherical $Fe_{76}Si_9B_{10}P_5$ amorphous powder made by gas atomization and $(NiZn)Fe_2O_4$ nanoparticles dispersed in epoxy resin are investigated in details. Scanning electron microscopy and energy-dispersive X-ray spectroscopy analysis revealed that the surface layer of the amorphous powder consisted of $(NiZn)Fe_2O_4$ nanoparticles and epoxy resin with uniform surface coverage. The samples composited with $(NiZn)Fe_2O_4$ nanoparticles have an significant enhancement of permeability in comparison with uncoated ones. The permeability of the composite cores at 20 kHz is 101 with the addition of 2 wt% $(NiZn)Fe_2O_4$ nanoparticles, which was increased 44% as compared with that of uncoated samples (70). In addition, it could be able to maintain a relatively low core loss of 1210 mW/cm^3 (B_m = 0.1 T, f = 100 kHz). The compound $Fe_{76}Si_9B_{10}P_5/(NiZn)Fe_2O_4$ soft magnetic composites with excellent soft magnetic properties provide great potential for expanding the application of various electronic components like low frequency filters, DC output chokes and resonant inductors.

1. Introduction

Fe-based amorphous alloys have attracted extensive attention due to their excellent soft magnetic properties, which can be used to fabricate the soft magnetic powder cores with high performance [1–4]. However, due to the poor glass forming ability (GFA) of traditional Fe-based amorphous alloys, most of Fe-based amorphous powder was fabricated by crushing the corresponding amorphous ribbons [5–8]. Fe-based amorphous powder prepared through such an approach has generally irregular corners and sharp edges, and thus hard to compact and insulate. The undesirability of electrical insulation for the edges and corners of the powder will increase magnetic core loss and lead to unstable performance of amorphous powder cores. Therefore spherical amorphous powder will be a great choice for electrical insulation in the preparation of amorphous soft magnetic composites (ASMCs). In our previous work, Fe-Si-B-P amorphous alloy with excellent soft magnetic properties and high GFA has been reported [9,10]. Therefore, the spherical amorphous powder can be hopefully prepared by gas atomization [11]. It will be more easily to form a uniform insulation coating layer on the surface of the spherical amorphous powder, and can reduce the core loss of ASMCs.

For high-frequency applications, it is necessary to improve the electrical resistivity of amorphous powder by adding a suitable electrical insulating material [12]. Insulating material can create a thin layer on the surface of $Fe_{76}Si_9B_{10}P_5$ powders and separate them from one another. Amorphous powders are usually insulated electrically from each other by an organic and/or inorganic insulation layer on the powder surface before cold pressing [13–16]. The addition of these nonmagnetic insulation materials will reduce the permeability and the saturation magnetization of the soft magnetic powder cores [17,18]. Therefore, it is not conducive to the miniaturization of electronic components. However, ferrites have unique properties such as very high electric resistivity, very low eddy current losses and relatively high magnetic permeability [19–21]. Thus, it should be an ideal insulating material for electrical insulation between amorphous powders and maintain the soft magnetic powder cores without any notable decrease in magnetic properties.

* Corresponding authors.
E-mail addresses: dongyq@nimte.ac.cn (D. Yaqiang), ctchang@nimte.ac.cn (C. Chuntao).

http://dx.doi.org/10.1016/j.jallcom.2016.11.241
0925-8388/

In this paper, spherical $Fe_{76}Si_9B_{10}P_5$ amorphous powder was successfully prepared by gas atomization. We have made carefully design on the insulation layer on the surface of amorphous powder and successfully realized the preparation of ASMCs by compositing spherical $Fe_{76}Si_9B_{10}P_5$ amorphous powder with nano-(NiZn)Fe_2O_4 particles which were dispersed in epoxy resin. With this idea, we can make the soft magnetic powder cores with better overall performance to applications in the medium and high frequency fields [22].

2. Experimental

2.1. Synthesis of $Fe_{76}Si_9B_{10}P_5$ amorphous powders particles by gas atomization

Multicomponent alloy ingots with compositions of $Fe_{76}Si_9B_{10}P_5$ were prepared by induction melting the mixtures of pure Fe metal (99.99 wt%), pure B (99 wt%) and Si (99.99 wt%) crystals, and pre-alloyed Fe-P (99 wt%) alloy in a purified argon atmosphere. Spherical $Fe_{76}Si_9B_{10}P_5$ amorphous powder was prepared by gas atomization. The $Fe_{76}Si_9B_{10}P_5$ ingots were remelted under vacuum in a quartz tube using an induction-heating coil, injected through a nozzle with a diameter of 0.8 mm and atomized by high-pressure argon gas with a dynamic pressure of 7 MPa.

2.2. Design of $Fe_{76}Si_9B_{10}P_5$ amorphous powder/(NiZn)Fe_2O_4 nanoparticles composite

Due to the small particle size, large specific surface area, higher specific surface energy, which belongs to the thermodynamic instability system, so the phenomenon of particle coagulation and agglomeration are very easy to occur in the process of preparation or application [23,24]. The traditional method of preparation of magnetic powder cores cannot solve the problem of nanoparticles agglomeration. When the amorphous powders were directly compounded with the (NiZn)Fe_2O_4 nanoparticles by the grinding method, the strength between them was not enough to be formed in the subsequent process of cold pressing. Ultrasonic treatment is an effective method to solve the problem of nanoparticles agglomeration [25,26]. We designed that the (NiZn)Fe_2O_4 nanoparticles were firstly dispersed evenly in the epoxy resin by ultrasonic, and then the epoxy resin was coated on the surface of amorphous powders. In this way, not only solved the problem of nanoparticle aggregation, but also the resin was provided with sufficient strength in the process of cold pressing.

2.3. Preparation of $Fe_{76}Si_9B_{10}P_5$ amorphous powder/(NiZn)Fe_2O_4 nanoparticles composite powder cores

The sieved $Fe_{76}Si_9B_{10}P_5$ amorphous powder with particle sizes below 75 μm were used to prepare the amorphous powder cores. In acetone solution, the (NiZn)Fe_2O_4 nanoparticles were dispersed in the epoxy resin by Ultrasonic cleaner for 10 min. The (NiZn)Fe_2O_4 nanoparticles have a purity of 99.9% and an average particle diameter of 30 nm, supplied by Deke New Materials Co. Ltd. Subsequently, the obtained amorphous powder was added to the acetone solution and continuously stirring with glass rod until the acetone solution volatile completely. The composite powder was then dried for 30 min in an electric thermostatic drying oven. Toroid-shaped $Fe_{76}Si_9B_{10}P_5$ amorphous powder cores with an outer diameter of 20.3 mm, an inner diameter of 12.7 mm and a height of 5.3 mm were fabricated by cold pressing under a pressure of 1600 MPa at room temperature. Then the compacted cores were annealed at 673 K for 1 h in vacuum atmosphere to reduce the internal stress caused by pressing. The $Fe_{76}Si_9B_{10}P_5$ amorphous powder cores without (NiZn)Fe_2O_4 nanoparticles coatings were also prepared under the same conditions for comparison.

2.4. Characterizations

The characteristics of the gas-atomized powder were analyzed by X-ray diffraction (XRD) using Cu Kα-radiation, differential scanning calorimetry (DSC) and scanning electron microscopy (SEM). The structure of the insulating layers on the surface of amorphous powder was characterized using SEM coupled with energy-dispersive X-ray spectroscopy (EDS). Permeability (μ) spectra were measured by an impedance analyzer (HP 4294A) from 1 kHz to 110 MHz with the contact electrodes in two-terminal connection configuration. Core loss of the soft magnetic powder cores was measured by an AC B–H loop tracer.

3. Results and discussion

3.1. The properties of $Fe_{76}Si_9B_{10}P_5$ amorphous powders

The XRD pattern of the $Fe_{76}Si_9B_{10}P_5$ powders was shown in the Fig. 1. As seen in this figure, only a diffuse halo pattern typical for an amorphous phase is seen, and no peak of a crystalline phase is observed. It indicates that a glassy phase without crystallinity is formed in the particle size range below 75 μm. Scanning electron microscope image shown in Fig. 1 as a topmost inset suggests that $Fe_{76}Si_9B_{10}P_5$ powder particles made by gas atomization method are spherical in shape. Spherical amorphous powder is more favorable for the uniform insulation coating, thereby reducing the eddy current loss between the powders. Therefore, the application of the amorphous composite magnetic powder cores in the middle and high frequency can be greatly improved.

Fig. 2 shows the typical DSC curves of the gas-atomized $Fe_{76}Si_9B_{10}P_5$ ribbon and powders with a heating rate of 0.67 K/s in an Ar atmosphere. The DSC curve of $Fe_{76}Si_9B_{10}P_5$ powders shows an endothermic peak due to the Curie transition, and a glass transition, followed by an extended supercooled liquid region and almost single-stage of crystallization process, which means that the simultaneous precipitation of many kinds of crystalline phase, in agreement with that of the corresponding glassy alloy ribbon [9,10]. No appreciable difference in T_c, T_g, T_x, ΔT_x, and crystallization process is observed between the melt-spun ribbon and powders. Thus,

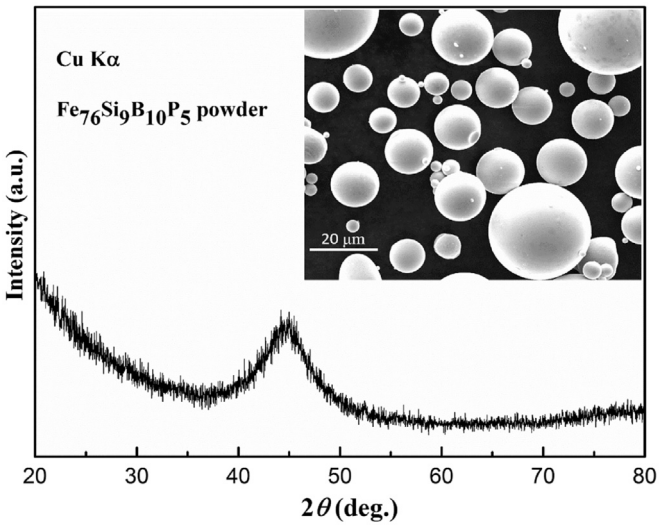

Fig. 1. XRD pattern and SEM image of the $Fe_{76}Si_9B_{10}P_5$ amorphous powders.

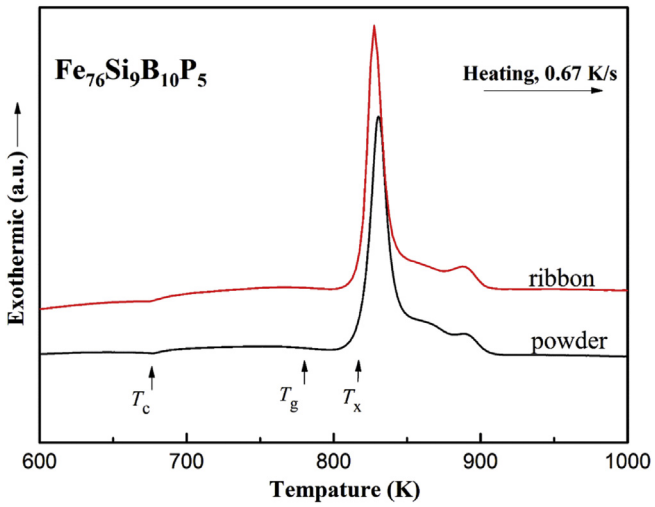

Fig. 2. DSC curves of $Fe_{76}Si_9B_{10}P_5$ ribbon and the gas atomized powder.

indicating that the $Fe_{76}Si_9B_{10}P_5$ powders made by gas atomization is completely amorphous [27].

3.2. Characterization of $Fe_{76}Si_9B_{10}P_5$ amorphous powder/(NiZn)Fe_2O_4 nanoparticles composite insulating layer

SEM micrographs and EDS analysis of the $Fe_{76}Si_9B_{10}P_5$ amorphous powder cores with (NiZn)Fe_2O_4 nanoparticle addition after polished were presented in Fig. 3. Elemental distribution maps of the cross-section of composite amorphous powder cores after curing were utilized to further characterize. It can be clearly seen that element Ni (purple color) and Zn (yellow color) lie mainly between the amorphous powder particles, and they almost exist in the same position. It indicates that (NiZn)Fe_2O_4 nanoparticles can be evenly dispersed in the epoxy resin by Sonication. Moreover, the $Fe_{76}Si_9B_{10}P_5$ amorphous powder are isolated from epoxy resin which modify by nano-(NiZn)Fe_2O_4 particles, which will improve the insulating property between the $Fe_{76}Si_9B_{10}P_5$ amorphous powders.

SEM micrograph of $Fe_{76}Si_9B_{10}P_5$ amorphous powder before (Fig. 4(a)) and after (Fig. 4(b)) being mixed with 2 wt% (NiZn)Fe_2O_4 nanoparticles were shown in Fig. 3. Apparently, epoxy resin mixed with (NiZn)Fe_2O_4 nanoparticles has completely and uniformly covered on the surface of the $Fe_{76}Si_9B_{10}P_5$ powders. It should be noticed that the addition of (NiZn)Fe_2O_4 nanoparticles does not cause any defects or structural imperfection in the homogeneous coating of epoxy resin on the surface of the amorphous powders, which is the key to ensure the relatively low eddy current loss of the amorphous powder cores. Moreover, the elemental distribution maps in the Fig. 4 reveal that Ni and Zn are uniformly distributed on the surface of the $Fe_{76}Si_9B_{10}P_5$ amorphous particles. A comparison of the coverage of Ni or Zn with that of Fe, Si, and P indicates that the (NiZn)Fe_2O_4 layer is thin [18]. Therefore, SEM and EDS elemental distribution maps demonstrate that the $Fe_{76}Si_9B_{10}P_5$ powders were coated by a uniform and thin insulating layer, which is composed of epoxy resin and (NiZn)Fe_2O_4 nanoparticles. The distinctive and outstanding insulating layer on the surface of amorphous powders is the key to fabricate ASMCs with excellent performance.

3.3. Magnetic properties of $Fe_{76}Si_9B_{10}P_5$ amorphous powders/(NiZn)Fe_2O_4 nanoparticles composite powder cores

It can be obviously seen from Fig. 5 that the permeability (μ) of composite powder cores has a great enhancement by adding (NiZn)Fe_2O_4 nanoparticles, and with the increase the content of (NiZn)Fe_2O_4 nanoparticles, the more μ increase. The μ at 20 kHz ranges from 70 to 112 for all the composite samples. The μ was determined from the inductance L_s of the ring samples using the following relations [23]:

$$\mu = \frac{L_s l_e}{\mu_0 N^2 A_e} \quad (1)$$

Where L_s is the inductance of the sample core, N *is* the total number of turns of the coil, μ_0 is the permeability of free space, A_e and l_e are the area of cross-section and the mean flux density path of the ring sample, respectively. The μ response of the samples can in general be explained in terms of different initial powders and their volume fraction. The μ strongly depends on the density, number of pores,

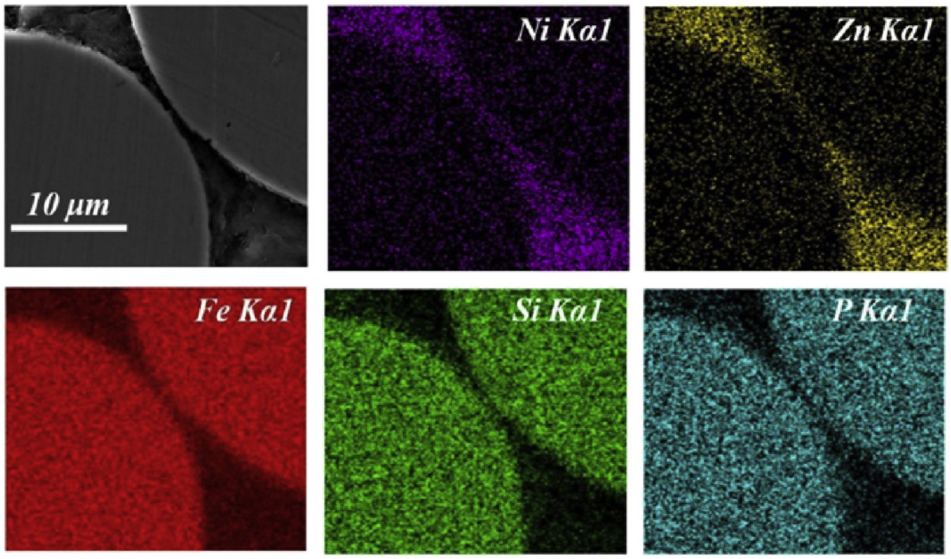

Fig. 3. SEM micrograph and EDS elemental distribution maps of the polished $Fe_{76}Si_9B_{10}P_5$/2 wt% (NiZn)Fe_2O_4 composite powder cores.

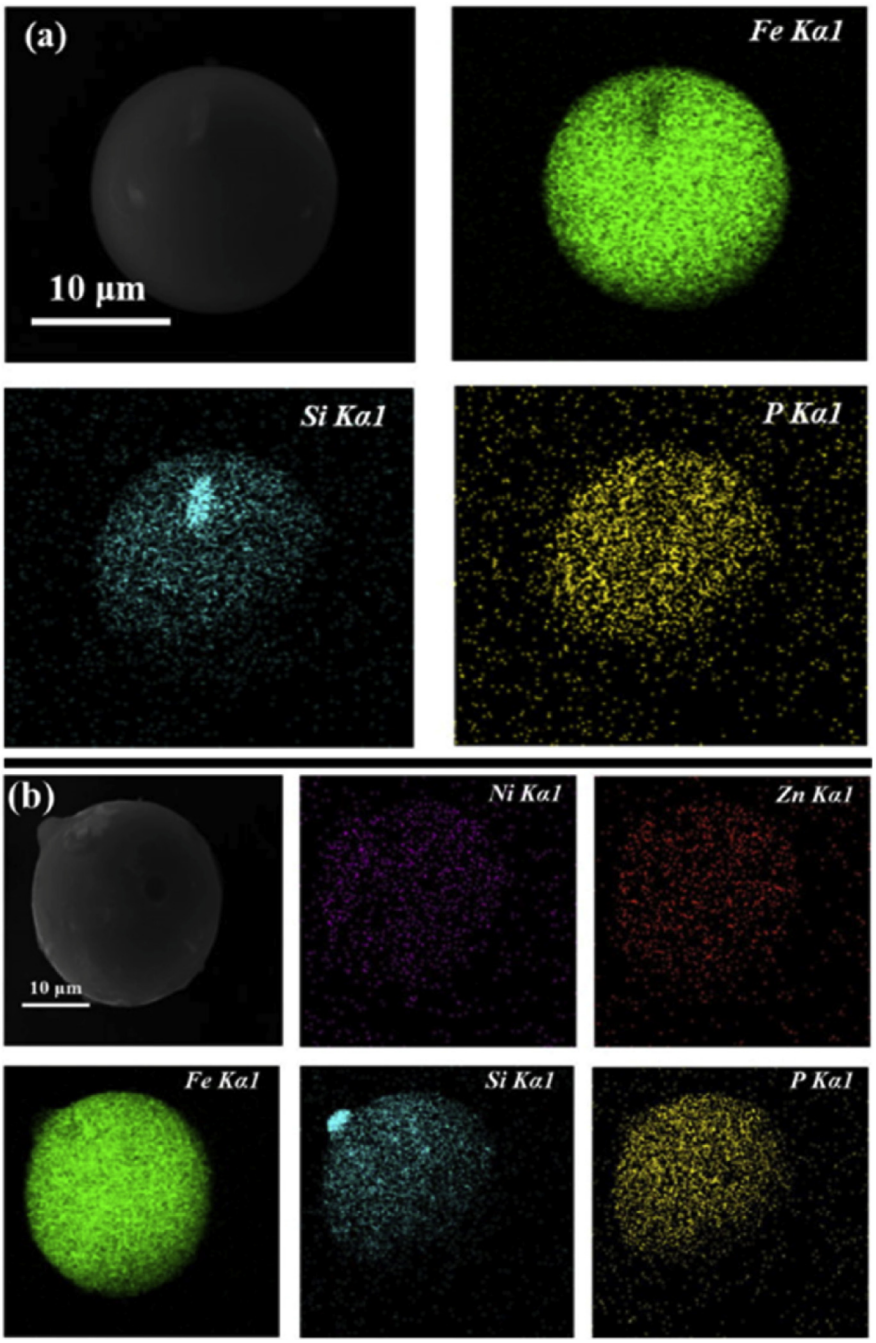

Fig. 4. SEM and EDS elemental distribution maps of $Fe_{79}Si_9B_{10}P_5$ powder being coated with (a) 0 wt % and (b) 2 wt% (NiZn)Fe_2O_4 nanoparticles respectively.

non-magnetic phase, and magnetic anisotropy [24]. These parameters can impress domain wall displacement and spin rotation. Two main types of magnetization processes may basically influence the magnetic behavior of solid-state materials. In general, the dispersions caused by domain wall displacements occur in radio-frequency range (below 10 MHz), and those caused by domain rotations often appear in the microwave range (100 MHz–10 GHz). The measured spectra in our composite samples were closely associated with the relaxation process of the domain wall motion [25,26]. It is believed that the large increase of μ is attributed to the $Fe_{76}Si_9B_{10}P_5$/(NiZn)Fe_2O_4 nanoparticles micro-cellular structure, such as both cell-body and cell-wall are ferromagnetic, the insulating cell-walls distribute uniformly and the high densification composite structure [27].

Fig. 6 shows the core loss versus frequency of $Fe_{76}Si_9B_{10}P_5$ amorphous composite powder cores at the induction level of 0.1 T with different content of (NiZn)Fe_2O_4 nanoparticles. From this figure, the total core losses (P_{cv}) of $Fe_{76}Si_9B_{10}P_5$ amorphous composite powder cores slightly increases with raising the (NiZn)Fe_2O_4 nanoparticles content from 0 to 3 wt%, which is not obvious relative to the increase in permeability. The core loss versus induction (B_m) of $Fe_{76}Si_9B_{10}P_5$ amorphous powder cores with different content of (NiZn)Fe_2O_4 nanoparticles at 50 kHz can be seen in Fig. 7. Similarly, with raising the (NiZn)Fe_2O_4 nanoparticles content, the P_{cv} of $Fe_{76}Si_9B_{10}P_5$ amorphous composite powder cores increased slightly. This has a great relationship with the composition of the

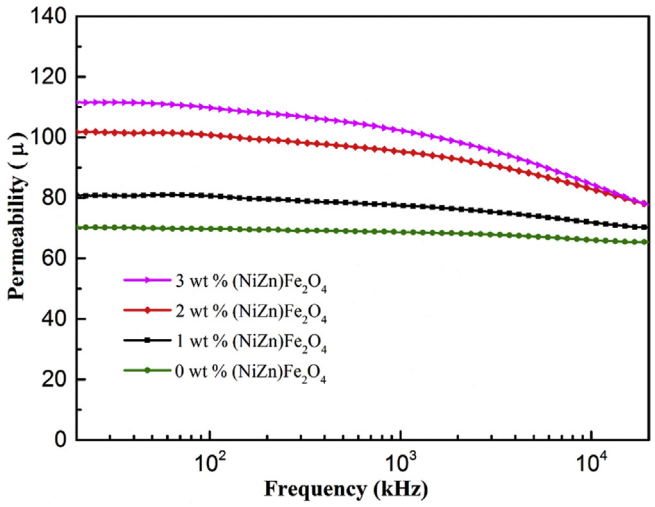

Fig. 5. Frequency dependence of the permeability for the $Fe_{76}Si_9B_{10}P_5$ amorphous powder cores with different content of $(NiZn)Fe_2O_4$ nanoparticles.

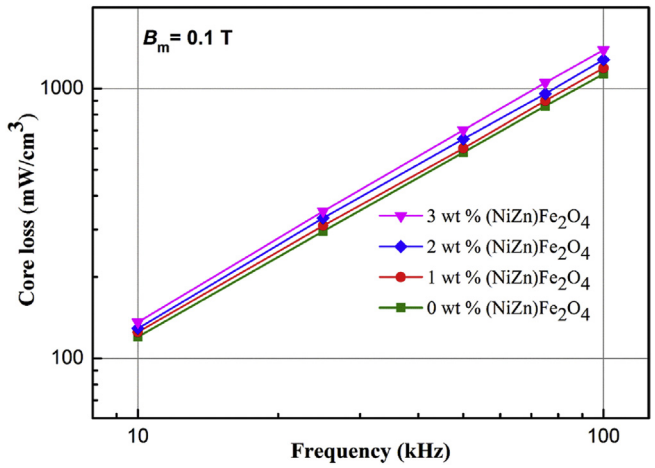

Fig. 6. Core loss versus frequency of $Fe_{76}Si_9B_{10}P_5$ amorphous powder cores with different content of $(NiZn)Fe_2O_4$ nanoparticles at the induction (B_m) level of 0.1 T.

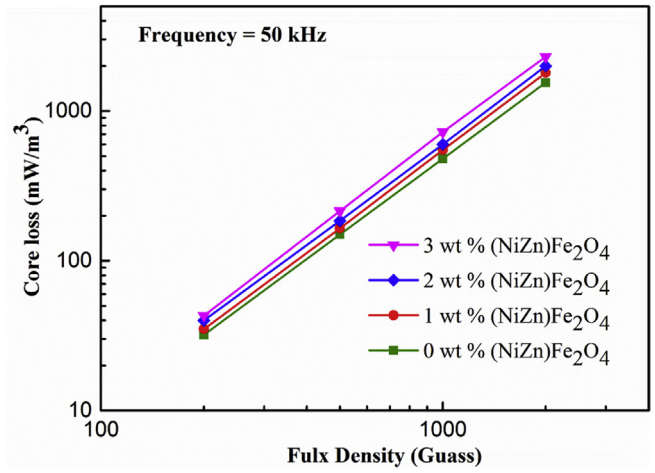

Fig. 7. Core loss versus induction (B_m) of $Fe_{76}Si_9B_{10}P_5$ amorphous powder cores with different content of $(NiZn)Fe_2O_4$ nanoparticles at 50 kHz.

core losses and the insulation coating process.

The total core losses (P_{cv}) can be represented by the following equation [14].

$$P_{cv} = P_h + P_e + P_a \tag{2}$$

In Eq. (2), P_h is the hysteresis loss, P_e is the eddy loss and P_a is the residual loss. Residual losses are a combination of relaxation and resonant losses. They are only important at very low induction levels and very high frequencies and can be ignored in power applications [14]. So the total core loss of a magnetic device is the sum of the eddy current losses and hysteresis losses.

At low frequencies the hysteresis loss is the main core loss part and can be reduced by large particle size, higher purity of the soft materials in the particles and stress relieving heat treatment. Hysteresis loss can be expressed as Eq. (3) [14]: [28].

$$P_h = f \oint HdB \tag{3}$$

In Eq. (3), f is the frequency, H is magnetic field intensity, and B is the flux density. The heat treatment procedure following the compaction is the main step to reduce hysteresis loss.

Eddy current loss is due to electrical resistance losses within the core caused by the alternating electric field. Eddy current loss can be described as Eq. (4) [14]: [29].

$$P_e = \frac{CB^2f^2d^2}{\rho} \tag{4}$$

In Eq. (4), C is the proportionality constant, B is the flux density, f is the frequency, ρ is the resistivity and d is the thickness of the material. The insulating coating of every particle gives very small eddy current paths inside a particle and a relatively high resistivity of the soft magnetic powder cores. The resistance of the ASMCs with the increase of nano-$(NiZn)Fe_2O_4$ is 9.68, 2.65, 1.29 and 0.982 MΩ respectively and has a slight decrease, but the overall resistance of the AMCs remains at a higher value (MΩ). This was one of the reasons for the little change on the core losses of the AMCs and the core losses can still maintain relatively low value. Another reason is that an excellent electro-insulating layer on the surface of $Fe_{76}Si_9B_{10}P_5$ amorphous powders consisted of $(NiZn)Fe_2O_4$ nanoparticles and epoxy resin have completely separated the $Fe_{76}Si_9B_{10}P_5$ amorphous powders from each other. That will decrease the eddy current loss between $Fe_{76}Si_9B_{10}P_5$ amorphous powders. In addition, although an extra addition of nano-$(NiZn)Fe_2O_4$ particles will increase the P_e and P_h of amorphous composite powder cores, but they have high electrical resistivity and the content is trace, so the contribution of $(NiZn)Fe_2O_4$ nanoparticles to the core losses is minor. Consequently, the P_{cv} of $Fe_{76}Si_9B_{10}P_5/(NiZn)Fe_2O_4$ composite powder cores can maintain relatively low value [8,9,30,31].

4. Conclusions

ASMCs based on $Fe_{76}Si_9B_{10}P_5$ amorphous powders and $(NiZn)Fe_2O_4$ nanoparticles dispersed in epoxy resin have been obtained. The homogeneous dispersion of soft magnetic nano-$(NiZn)Fe_2O_4$ particles has greatly improved the permeability of the amorphous composite powder cores. When the $(NiZn)Fe_2O_4$ nanoparticles content reached 3 wt%, the permeability of the composite powder cores increased markedly from 70 to 112, and the total core loss can be maintained at a relatively low standard. The unique insulation coating of $Fe_{76}Si_9B_{10}P_5$ amorphous composite materials provide us with valuable inspiration to develop new Fe-based amorphous powder cores with excellent magnetic properties of high permeability and relatively low core losses.

Acknowledgement

The work was supported by Ningbo Municipal Nature Science Foundation (Grant No. 2015A610008); Equipment Project for Research of the Chinese Academy of Sciences (Grant No. yz201434); Ningbo International Cooperation Projects (Grant No. 2015D10022); Ningbo Major Project for Science and Technology (Grant No. 2014B11012) and National Natural Science Foundation of China (Grant No. 51601205 and 51671206). Zhejiang Province Public Technology Research and Industrial Projects (2016C31025).

References

[1] T. Egami, P.J. Flanders, C.D. Graham, AIP Publishing. 24 (1975) 697–701.
[2] D. Raybould, K.S. Tan, J. Mater. Sci. 20 (1985) 2776–2786.
[3] S.F. Chen, C.Y. Chen, C.S. Cheng, J. Alloys Compd. 644 (2015) 17–24.
[4] B.V. Neamţu, T.F. Marinca, I. Chicinaş, O. Isnard, F. Popa, P. Păşcuţă, J. Alloys Compd. 600 (2014) 1–7.
[5] J. Füzer, S. Dobák, P. Kollár, J. Alloys Compd. 628 (2015) 335–342.
[6] H.J. Kim, S.K. Nam, K.S. Kim, S.C. Yoon, K.Y. Sohn, M.R. Kim, S.S. Yong, W.P. Won, Jpn. J. Appl. Phys. 51 (2012), 103001(1-3).
[7] E.A. Périgo, S. Nakahara, Y.Y. Pittini, H.Y. De, T. Graule, J. Magn. Magn. Mater 323 (2011) 1938–1944.
[8] X.Y. Wang, Z.H. Lu, C.W. Lu, G.M. Li, D.R. Li, J. Iron Steel Res. Int. 21 (2014) 1055–1058.
[9] C.T. Chang, C.L. Qin, A. Makino, A. Inoue, J. Alloys Compd. 533 (2012) 67–70.
[10] A. Makino, T. Kubota, M. Makabe, C.T. Chang, A. Inoue, Mater. Sci. Eng. B 148 (2008) 166–170.
[11] Z.K. Zhao, C.T. Chang, A. Makino, A. Okubo, A. Inoue, Mater. Trans. 50 (2009) 487–489.
[12] L.P. Lefebvre, S. Pelletier, C. Gelinas, J. Magn. Magn. Mater 176 (1997) L93–L96.
[13] X.Y. Wang, F. Guo, C.W. Lu, Z.H. Lu, D.R. Li, S.X. Zhou, J. Magn. 16 (2011) 318–321.
[14] H. Shokrollahi, K. Janghorban, J. Mater. Process. Tech. 189 (2007) 1–12.
[15] Y.B. Kim, D.H. Jang, H.K. Seok, K.Y. Kim, Mater. Sci. Eng. B 449–451 (2007) 389–393.
[16] A.H. Taghvaei, H. Shokrollahi, K. Janghorban, Mater. Des. 31 (2010) 142–148.
[17] Y.D. Peng, J.W. Nie, W.J. Zhang, J. Ma, C.X. Bao, Y. Cao, J. Magn. Magn. Mater 399 (2016) 88–93.
[18] X.A. Fan, Z.Y. Wu, G.Q. Li, J. Wang, Z.D. Xiang, Z.H. Gan, Mater. Des. 89 (2016) 1251–1258.
[19] S. Wu, A.Z. Sun, Z.W. Lu, C. Cheng, X.X. Gao, J. Magn. Magn. Mater 381 (2015) 451–456.
[20] W. Yan, W. Jiang, Q.H. Zhang, Y.G. Li, H.Z. Wang, Mater. Sci. Eng. B 171 (2010) 144–148.
[21] V.S. Yáñez, A.M. Sánchez, A.C. Gómez, J. Mira, R.M.A. Señarís, G.S. Castro, J. Solid State Chem. 182 (2009) 2685–2690.
[22] A.M. Leary, P.R. Ohodnicki, M.E. Mchenry, Jom 64 (2012) 772–781.
[23] G.Q. Lin, Z.W. Li, L. Chen, Y.P. Wu, C.K. Ong, J. Magn. Magn. Mater. 305 (2006) 291–295.
[24] A.H. Taghvaei, H. Shokrollahi, M. Ghaffari, K. Janghorban, J. Phys. Chem. Solids 71 (2010) 7–11.
[25] R. Valenzuela, Phys. B 299 (2001) 280–285.
[26] H. Shokrollahi, K. Janghorban, J. Magn. Magn. Mater 313 (2007) 182–186.
[27] A. Chevalier, F.M. Le, J. Appl. Phys. 90 (2001) 3462–3645.
[28] P. Kollár, Z. Birčáková, J. Füzer, R. Bureš, M. Fáberová, J. Magn. Magn. Mater. 327 (2013) 146–150.
[29] A.H. Taghvaei, H. Shokrollahi, K. Janghorban, H. Abiri, Mater. Desi 30 (2009) 3989–3995.
[30] J.J. Guo, Y.Q. Dong, Q.K. Man, Q. Li, C.T. Chang, C. Xin-Min Wang, R.W. Li, J. Magn. Magn. Mater 401 (2016) 432–435.
[31] M. Streckova, J. Fuzerb, L. Medvecky, R. Bures, P. Kollar, M. Faberov, V. Girman, B. Mater Sci. 37 (2014) 167–177.